# The Origin of the Kink Phenomenon of Transistor Scattering Parameter $S_{22}$

Shey-Shi Lu, *Senior Member, IEEE*, Chinchun Meng, To-Wei Chen, and Hsiao-Chin Chen

***Abstract*—A novel theory based on dual-feedback circuit methodology is proposed to explain the kink phenomenon of transistor scattering parameter $S_{22}$. Our results show that the output impedance of *all* transistors intrinsically shows a *series RC* circuit at low frequencies and a *parallel RC* circuit at high frequencies. It is this inherent ambivalent characteristic of the output impedance that causes the appearance of kink phenomenon of $S_{22}$ in a Smith chart. It was found that an increase of transistor transconductance enhances the kink effect while an increase of drain-to-source (or collector-to-emitter) capacitance obscures it. This explains why it is much easier to see the kink phenomenon in bipolar transistors, especially heterojunction bipolar transitors, rather than in field-effect transistors (FETs). It also explains why the kink phenomenon is seen in larger size FETs and not in smaller size FETs. Our model not only can predict the behavior of $S_{22}$, but also calculate all $S$-parameters accurately. Experimental data of submicrometer gate Si MOSFETs and GaAs FETs are used to verify our theory. A simple method for extracting transistor equivalent-circuit parameters from measured $S$-parameters is also proposed based on our theory. Compared with traditional $Z$- or $Y$-parameter methods, our theory shows another advantage of giving deep insight into the physical meaning of $S$-parameters.**

***Index Terms*—BJT, FET, HBT, kink phenomenon, MOSFET, $S$-parameters.**

## I. Introduction

TRANSISTOR scattering parameters ($S$-parameters) have been used extensively in active microwave circuit design. However, some behaviors of transistor $S$-parameters are still not fully understood. For example, the kink phenomenon of the scattering parameter $S_{22}$ in a Smith chart, such as shown in Fig. 1 [1], has been a puzzle for a long time. This is because it was thought that $S_{22}$ should roughly follow a constant conductance circle in the Smith chart instead of the shape, as shown in Fig. 1. Furthermore, it is strange that this kink phenomenon is invisible when the device size of an FET is small, but only becomes apparent in a large device. In addition, this kink effect is much more frequently seen in bipolar transistors, especially heterojunction bipolar transistors (HBTs), as compared with FETs. Traditionally, transistor $S$-parameters are mostly understood in terms of $Y$- or $Z$-parameters. These $Y$- or $Z$-parameters, though very useful in calculating $S$-parameters, cannot provide insight into the behavior or physical meaning of the $S$-parameters. For instance, it is difficult for $Y$- or $Z$-parameters to describe the frequency response of $S$-parameters directly or to explain the kink behavior of $S_{22}$ mentioned above.

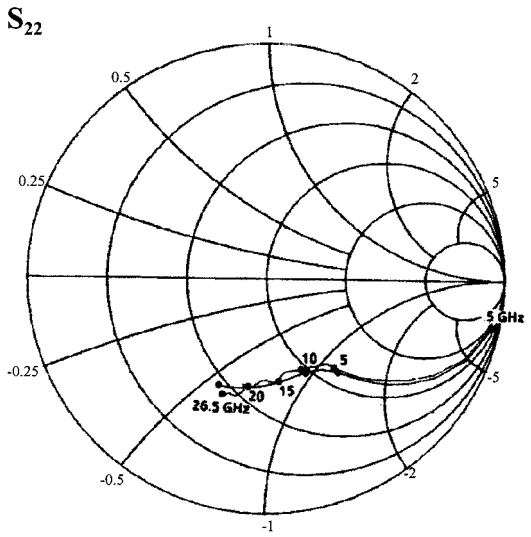


Fig. 1. Kink phenomenon of $S_{22}$ of an HBT observed in a Smith chart.

In this paper, we present a novel theory to explain these mysterious characteristics by deriving the output impedance (or admittance) of a transistor under the measurement conditions of $S$-parameters. In the derivation, the concept of dual feedback was employed to simplify the circuit analysis. The output impedance (or admittance) is different from $Z$-parameters (or $Y$-parameters) in that it is measured under the condition that the input and output ports of the transistors are connected with 50 $\Omega$ instead of an open or short circuit. By observing the behavior of the output impedance (or admittance) at both high and low frequencies, the kink phenomenon can be easily explained. We have found that the calculated values of $S_{22}$ for submicrometer gate GaAs FETs with different gate width by our theory agree well with the experimental data. To further verify our proposed method, we have also applied the above-mentioned method to obtain the other three $S$-parameters, i.e., $S_{11}$, $S_{21}$, and $S_{12}$, and compared them with other experimental results of 0.25-$\mu$m gate Si MOSFETs. Excellent agreement between theoretical values and experimental data was found. Our theory has the advantage of giving insight into the physical meaning of the $S$-parameters much more easily and clearly.

Manuscript received September 17, 1999. This paper was supported under Contract 89-E-FA06-2-4, under Contract NSC88-2219E-002-044, and under Contract NSC88-2219-E-005-003.

S.-S. Lu, T.-W. Chen, and H.-C. Chen are with the Department of Electrical Engineering, National Taiwan University, Taipei, Taiwan 10617, R.O.C. (e-mail: sslu@cc.ee.ntu.edu.tw).

C. Meng is with the Department of Electrical Engineering, Chung-Hsing University, Taichung, Taiwan 40227, R.O.C.

Publisher Item Identifier S 0018-9480(01)01074-2.

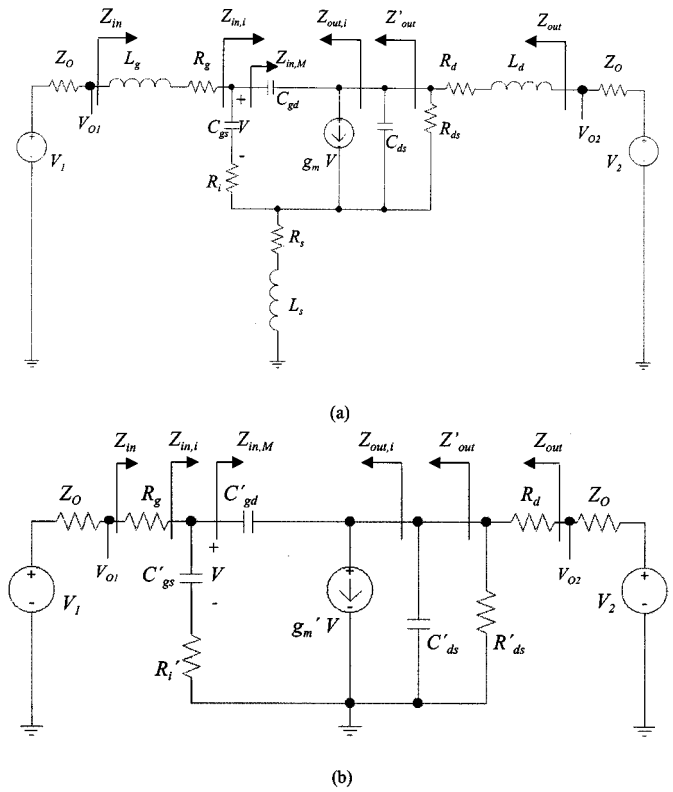


Fig. 2. Setup for the measurement of transistor $S$-parameters. (a) Complete circuit. (b) Simplified circuit with the local series–series feedback element ($R_S$) absorbed.

## II. Theory

The setup for the measurement of transistor $S$-parameters is shown in Fig. 2(a), where $Z_O(=1/Y_O)=50\ \Omega$ is connected to the input and output ports of the device-under-test. $S_{11}$ and $S_{21}$ can be measured by setting $V_2=0$ and $V_1\neq 0$, while $S_{22}$ and $S_{12}$ can be measured by setting $V_1=0$ and $V_2\neq 0$. Let us consider $S_{22}$ first. If the expression for the output impedance $Z_{\rm out}$ of this circuit has been found, then $S_{22}$ is given by

$$S_{22}=\frac{Z_{\rm out}-Z_O}{Z_{\rm out}+Z_O}. \tag{1}$$

This circuit configuration, in general, is too complicated to find its output impedance. Nevertheless, if this circuit is viewed as a dual feedback circuit in which $R_S$ is the local series–series feedback element and $C_{\rm gd}$ is the local shunt–shunt feedback element, then the problem becomes much more tractable. For simplicity, all the inductors in Fig. 2(a) are temporarily neglected. We will refer to them in later discussions in Section III. From local series–series feedback theory [2], the circuit of Fig. 2(a) can be transformed into that of Fig. 2(b) with some necessary circuit element modifications as follows:

$$C'_{\rm gs}=\frac{C_{\rm gs}}{1+g_mR_S} \tag{2}$$

$$R'_i=R_i+R_S \tag{3}$$

$$C'_{\rm ds}=\frac{C_{\rm ds}}{1+g_mR_S} \tag{4}$$

$$R'_{\rm ds}=R_{\rm ds}\cdot(1+g_mR_S) \tag{5}$$

$$C'_{\rm gd}=C_{\rm gd} \tag{6}$$

$$g'_m=\frac{g_m}{1+g_m\cdot R_S} \tag{7}$$

where $g_m=g_{mo}\cdot\exp(-j\omega\tau)$ and $g_{mo}$ is the dc transconductance and all the other symbols have their usual meaning. Except for some minor second-order correction terms, (2)–(7) are basically the same as those derived by Minasian [3] from a direct comparison of the $Y$-parameters between the circuits of Fig. 2(a) and Fig. 2(b).

Now the circuit in Fig. 2(b) is much easier to handle. For the convenience of discussing the origin of kink phenomenon, we define an "intrinsic output impedance" $Z_{{\rm out},i}$ seen to the left-hand side of the drain-to-source capacitance $C'_{\rm ds}$ (or $C_{\rm ds}$). By intrinsic, we mean that this output impedance does not include $R_{\rm ds}$, $R_d$, and $C_{\rm ds}$ in FETs (or $R_{\rm ce}$, $R_c$, and $C_{\rm ce}$ in bipolar junction transistors (BJTs) or HBTs) and is different from the normally defined output impedance $Z_{\rm out}$ seen to the left-hand side of $Z_O$ and $V_2$, as indicated in Fig. 2. The expression of the intrinsic impedance can easily be obtained from local shunt–shunt theory [2] and is given by

$$\begin{aligned}Z_{{\rm out},i}&=\frac{\left(sC''_{\rm gs}+\dfrac{1}{Z_{O1}}\right)^{-1}+\dfrac{1}{sC''_{\rm gd}}}{1+g''_m\left(sC''_{\rm gs}+\dfrac{1}{Z_{O1}}\right)^{-1}}\\&=\frac{1+s(C''_{\rm gs}+C'_{\rm gd})Z_{O1}}{(1+g''_mZ_{O1})sC'_{\rm gd}+s^2C''_{\rm gs}C'_{\rm gd}}\end{aligned} \tag{8}$$

where $C''_{\rm gs}=C'_{\rm gs}/(1+sR'_iC'_{\rm gs})$, $g''_m=g'_m/(1+sR'_iC'_{\rm gs})$, and $Z_{O1}=Z_O+R_g$. Once this intrinsic output impedance is known, the normal output impedance is nothing but the parallel combination of $Z_{{\rm out},i}$, $C'_{\rm ds}$, and $R'_{\rm ds}$ followed by a series combination with $R_d$ as follows:

$$Z_{\rm out}=Z_{{\rm out},i}\left\|\frac{1}{sC'_{\rm ds}}\right\|R'_{\rm ds}+R_d. \tag{9}$$

Here, the symbol $\|$ represents parallel combination. From (9), $S_{22}$ can be determined according to (1). We will discuss more about the properties of $Z_{{\rm out},i}$ and $S_{22}$ in Section III. We now turn our attention to $S_{11}$. According to local shunt–shunt feedback theory [2], it can be easily proven that the input impedance $Z_{{\rm in},M}$ seen to the right-hand side of $C'_{\rm gs}$ and $R'_i$ (or $C_{\rm gs}$ and $R_i$) is given by

$$Z_{{\rm in},M}=\frac{\dfrac{1}{sC'_{\rm gd}}+Z_L}{1+g''_mZ_L}=\frac{1}{s(1+g''_mZ_L)C'_{\rm gd}}+\frac{Z_L}{1+g''_mZ_L} \tag{10}$$

where $Z_L$ is the parallel combination of $Z_O+R_d$, $R'_{\rm ds}$, and $C'_{\rm ds}$. In fact, (10) reduces to the impedance of the Miller capacitance under the special case of negligibly small $C'_{\rm ds}$ and sufficiently large $g''_m$. From (10), $S_{11}$ can be determined by

$$S_{11}=\frac{Z_{\rm in}-Z_O}{Z_{\rm in}+Z_O}=\frac{R_g+Z_{{\rm in},i}-Z_O}{R_g+Z_{{\rm in},i}+Z_O} \tag{11}$$

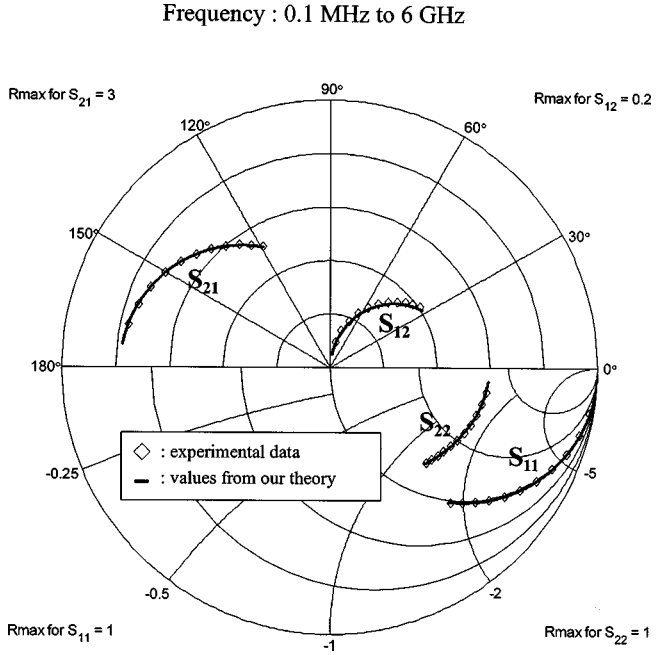


Fig. 3. Comparison of the experimental and calculated $S$-parameters of a 0.25-$\mu$m-gate Si MOSFET. Diamonds (◇): experimental data, solid line (—): calculated values by our theory.

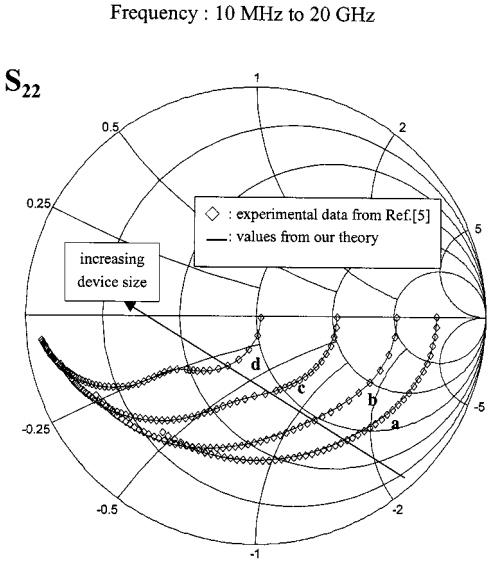


Fig. 4. Comparison of the experimental and calculated $S_{22}$ of submicrometer gate GaAs FETs with different gate width. Diamonds (◇): experimental data, solid line (—) : calculated values by our theory. Gate width: $a$: 0.5 mm, $b$: 1 mm, $c$: 2 mm, $d$: 4 mm. Note that the kink phenomenon becomes visible as the gate width is increased.

where $Z_{\rm in} = R_g + Z_{{\rm in},\,i}$ and $Z_{{\rm in},\,i} = [Z_{{\rm in},\,M} \| (R_i' + 1/sC_{\rm gs}'')]$ is the input impedance seen to the right-hand side of $R_g$.

As for $S_{21}$, the physical meaning of it is twice the voltage gain $V_{O2}/V_1$. Hence, it can easily be expressed in terms of $Z_{{\rm in},\,i}$, $g_m''$, $C_{\rm gd}'$, $R_d$, $R_g$, $Z_L$, and $Z_O$ as follows:

$$S_{21} = -2 \cdot \frac{Z_{{\rm in},\,i}}{Z_O + R_g + Z_{{\rm in},\,i}} \cdot (g_m'' - sC_{\rm gd}') \cdot \frac{Z_L \cdot \dfrac{1}{sC_{\rm gd}'}}{Z_L + \dfrac{1}{sC_{\rm gd}'}} \cdot \frac{Z_O}{Z_O + R_d}. \quad (12)$$

The physical meaning of $S_{12}$, on the other hand, is twice the reverse voltage gain $V_{O1}/V_2$. It is given as follows by inspecting Fig. 2(b):

$$S_{12} = 2 \frac{Z_{{\rm out},\,i} \| R_{\rm ds}' \| \dfrac{1}{sC_{\rm ds}'}}{Z_{{\rm out},\,i} \| R_{\rm ds}' \| \dfrac{1}{sC_{\rm ds}'} + R_d + Z_O} \cdot \frac{sC_{\rm gd}'}{sC_{\rm gd}' + sC_{\rm gs}'' + \dfrac{1}{Z_O + R_g}} \cdot \frac{Z_O}{Z_O + R_g}. \quad (13)$$

## III. Eperimental Results and Discussion

To verify our theory, we have applied (1)–(13) to a 0.25-$\mu$ m-gate MOSFET [4] in the calculations of its $S$-parameters. The effect of inductors in Fig. 2(a), which we neglected previously in Section II, can be easily included by replacing $R_g$, $R_S$, and $R_d$ with $R_g + j\omega L_g$, $R_S + j\omega L_s$, and $R_d + j\omega L_d$, respectively. Excellent agreement between the calculated values and experimental results is found (Fig. 3). Note that there is no visible kink phenomenon in Fig. 3 because the device size (10 $\mu$m) of the FET is too small. The kink effect will gradually become visible when the device size is increased, as was demonstrated experimentally by Aoki and Hirano [5] in Fig. 4. The reason for the enhancement will become clear after the following discussion.

In order to explore the origin of the kink phenomenon observed in Fig. 1 for HBTs and in Fig. 4 for FETs, (8) for the intrinsic output impedance has to be reexamined more closely. To get more insight into (8), let us assume that $R_i'$ is negligibly small, which is usually the case. The general behavior of (8) will not be affected much by neglecting $R_i'$. Under this assumption, (8) is equal to

$$Z_{{\rm out},\,i} = \frac{1 + s(C_{\rm gs}' + C_{\rm gd}')Z_{O1}}{(1 + g_m' Z_{O1}) sC_{\rm gd}' + s^2 C_{\rm gs}' C_{\rm gd}'}. \quad (14)$$

Plugging $s = j\omega$ into (14) and after some simple mathematical manipulation, we find that, at high frequencies, $Z_{{\rm out},\,i}$ approaches a *parallel RC* network with conductance $g = Y_{O1}(C_{\rm gd}'/C_{\rm gs}' + C_{\rm gd}')^2 + g_m' C_{\rm gd}'/(C_{\rm gs}' + C_{\rm gd}')$ and capacitance $C_p = C_{\rm gs}' C_{\rm gd}'/(C_{\rm gs}' + C_{\rm gd}')$, while at low frequencies, it can be approximated by a *series RC* network with resistance $r = Z_{O1}/(1 + g_m' Z_{O1}) + g_m' C_{\rm gs}'/[(Y_{O1} + g_m')^2 C_{\rm gd}']$ and capacitance $C_s = (1 + g_m' Z_{O1}) C_{\rm gd}'$, where $Y_{O1}$ is the inverse of $Z_{O1}$. That is, at high frequencies

$$\begin{aligned} Y_{{\rm out},\,i} &= \frac{1}{Z_{{\rm out},\,i}} \\ &\approx \left[ Y_{O1} \left( \frac{C_{\rm gd}'}{C_{\rm gs}' + C_{\rm gd}'} \right)^2 + g_m' \frac{C_{\rm gd}'}{C_{\rm gs}' + C_{\rm gd}'} \right] + \frac{1}{j\omega \dfrac{C_{\rm gs}' C_{\rm gd}'}{C_{\rm gs}' + C_{\rm gd}'}} \\ &\approx g + sC_p \end{aligned} \quad (15)$$

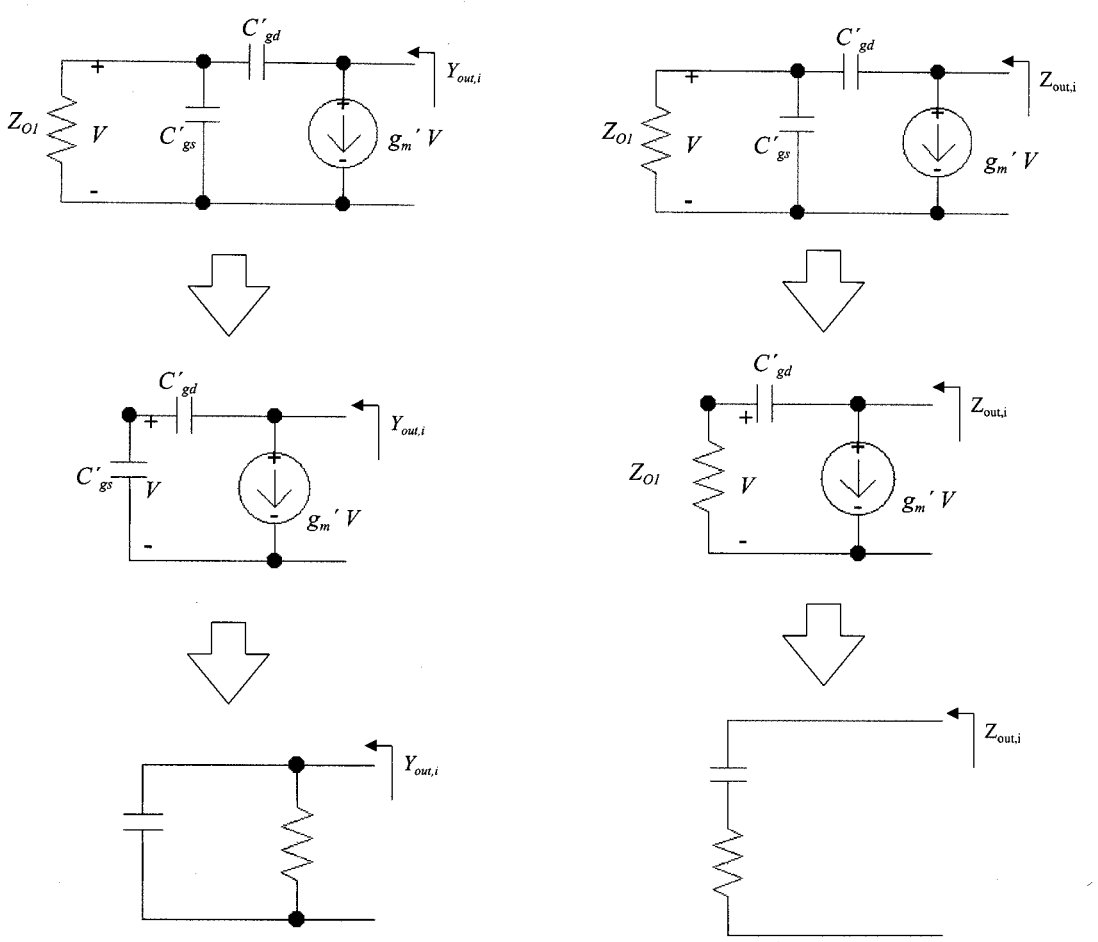


Fig. 5. Equivalent circuit of the intrinsic output impedance/admittance. (a) At high frequencies: the intrinsic output admittance approaches a parallel *RC* circuit. (b) At low frequencies: the intrinsic output impedance can be approximated by a series *RC* circuit.

while at low frequencies

$$Z_{\text{out},i} = \frac{1 + j\omega(C'_{\text{gs}} + C'_{\text{gd}})Z_{O1}}{(1 + g'_m Z_{O1})j\omega C'_{\text{gd}} - \omega^2 C'_{\text{gs}} C'_{\text{gd}}}$$
$$\approx \left( \frac{Z_{O1}}{1 + g'_m Z_{O1}} + \frac{g'_m}{(Y_{O1} + g'_m)^2} \cdot \frac{C'_{\text{gs}}}{C'_{\text{gd}}} \right) + \frac{1}{j\omega(1 + g'_m Z_{O1})C'_{\text{gd}}}$$
$$\approx r + \frac{1}{j\omega C_s}. \tag{16}$$

The results of (15) and (16) are very reasonable from the physical point-of-view and can be qualitatively understood as follows. Compared with $C'_{\text{gs}}$, $Z_{O1}(= Z_O + R_g)$ can be thought of as an open circuit at very high frequencies. The total capacitance is thus the series combination of $C'_{\text{gs}}$ and $C'_{\text{gd}}$, thus, the current source can be replaced by a conductance determined by the ratio of the $C'_{\text{gs}}$ and $C'_{\text{gd}}$ capacitive voltage divider. Therefore, the resultant circuit is a *parallel RC* circuit, as is illustrated in Fig. 5(a). On the other hand, at low frequencies, $C'_{\text{gs}}$ compared with $Z_{O1}$ can be treated as open circuit so that $Z_{O1}$ is in series with $C'_{\text{gd}}$. It can be easily proven that the final result of this parallel combination of the dependent current source and the *series RC* circuit is again a series *RC* circuit, as illustrated in Fig. 5(b).

The trends predicted by (15) and (16) have been verified in Fig. 6, where the data points have been calculated from (14)–(16). As can clearly be seen from Fig. 6, the intrinsic output impedance indeed follows a constant resistance circle at low frequencies and then a constant conductance circle at high frequencies. It is this inherent ambivalent characteristic of the intrinsic output impedance (or admittance) that causes the appearance of the kink phenomenon of $S_{22}$ in a Smith chart. Also shown in Fig. 6 is the effect of $R'_{\text{ds}}$ (or $R_{\text{ds}}$). Basically, $R'_{\text{ds}}$ only changes the starting point of $S_{22}$ on the real axis from the open-circuit point to a point where the resistance is equal to approximately $R'_{\text{ds}}$. That is, $R'_{\text{ds}}$ only distorts the shape of $S_{22}$ and does not affect the appearance of the kink phenomenon. Therefore, from now on we will disregard the effect of $R'_{\text{ds}}$. From the above discussion, we also conclude that the kink phenomenon of $S_{22}$ is an inherent property in *all* transistors and that the kink point or dip point should happen approximately at the intercept point of the constant resistance ($r$) circle and the constant conductance ($g$) circle.

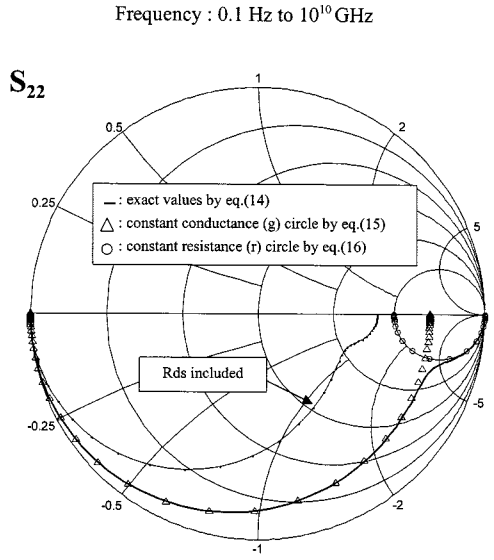


Fig. 6. Kink phenomenon of $S_{22}$ in the Smith chart due to the ambivalent characteristic of the intrinsic transistor output impedance. $R_{\rm ds}$ only changes the starting point of $S_{22}$ and does not affect the appearance of the kink phenomenon. Circles (◯) were calculated by (16) (constant resistance circle) and triangles (△) were calculated by (16) (constant conductance circle). Both cases agree well with the solid line (—) calculated by the exact formula (14) at both high and low enough frequencies, respectively.

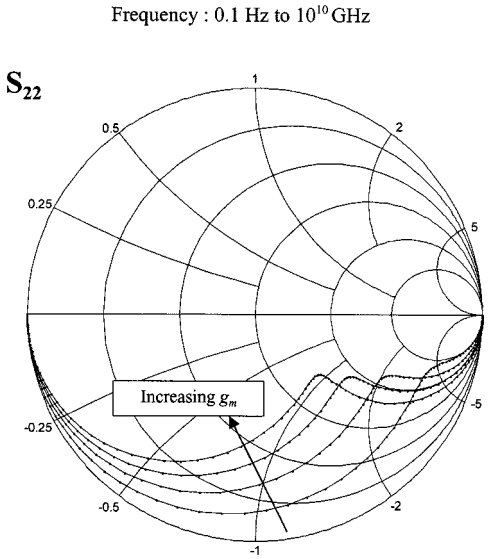


Fig. 7. Effect of $g_m$ on the kink phenomenon of $S_{22}$. The kink phenomenon becomes more pronounced as $g_m$ is increased because the intercept point of the constant resistance circle and the constant conductance circle moves to a new point with smaller resistance and larger conductance.

If $g'_m$ (or $g_m$) is increased, then from (15) and (16), $r$ decreases and $g$ increases and, hence, the kink point moves to a new intercept point with smaller $r$ and larger $g$, which makes the kink phenomenon looking more pronounced, as shown in Fig. 7. This is one reason why it is much easier to see the kink effect in bipolar transistors than in FETs because bipolar transistors usually show larger $g_m$ than FETs.

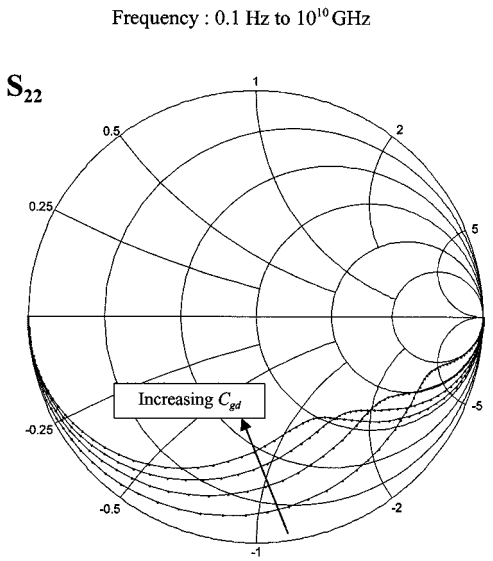


Fig. 8. Effect of $C_{\rm gd}$ on the kink phenomenon of $S_{22}$. The effect of $C_{\rm gd}$ is similar to that of $g_m$.

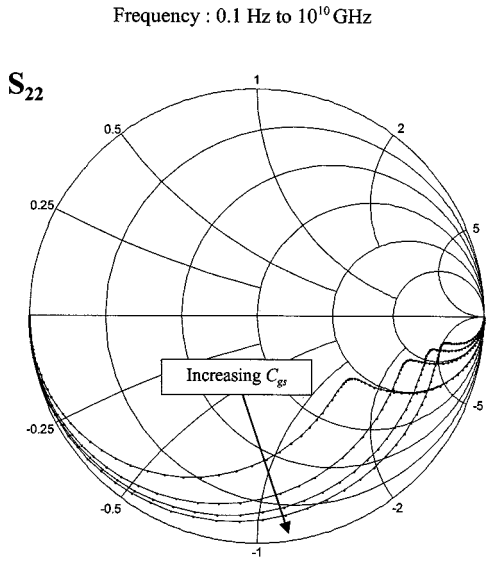


Fig. 9. Effect of $C_{\rm gs}$ on the kink phenomenon of $S_{22}$. The kink point moves to a point with larger resistance and smaller conductance.

If $C'_{\rm gd}$ (or $C_{\rm gd}$) is increased, then again from (15) and (16), $r$ decreases and $g$ increases and the effect of $C'_{\rm gd}$ on the kink phenomenon (see Fig. 8) is similar to that of $g'_m$.

On the other hand, $r$ increases and $g$ decreases as $C'_{\rm gs}$ is increased and, thus, the kink point moves to a point closer to the open circuit point, as shown in Fig. 9.

Next, let us consider how $C'_{\rm ds}$ (or $C_{\rm ds}$) influences the kink phenomenon. If the effect of $C'_{\rm ds}$ is added to the intrinsic output impedance $Z_{{\rm out},i}$ (or admittance $Y_{{\rm out},i} = 1/Z_{{\rm out},i}$), it can be easily shown that the total admittance $Y'_{\rm out}$ seen to the left-hand side of $R'_{\rm ds}$ at high frequencies is still a parallel *RC* circuit with

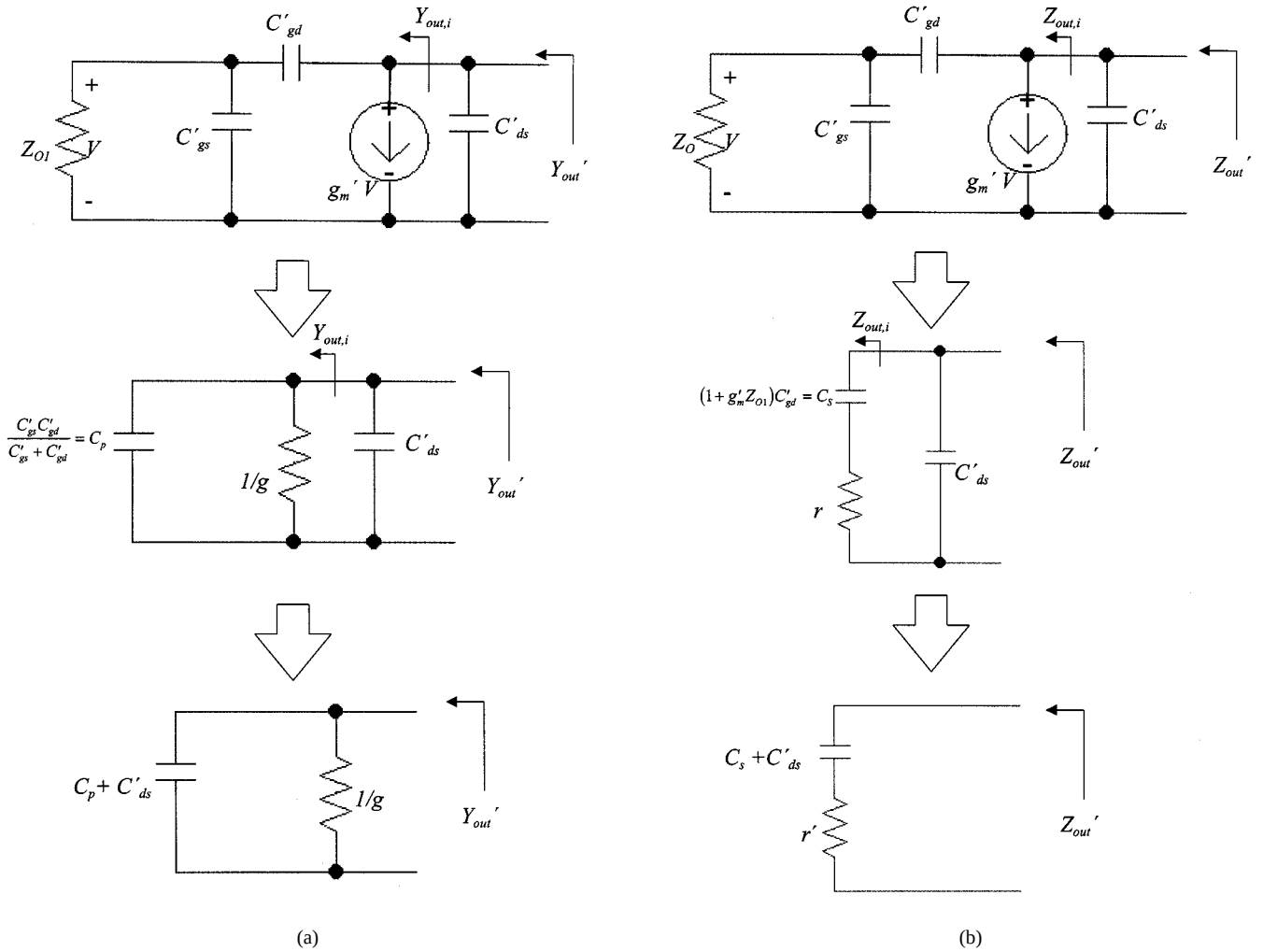


Fig. 10. Effect of the addition of $C'_{\rm ds}$ to the intrinsic output impedance. (a) At high frequencies, the resultant output impedance is still a parallel *RC* circuit with an unchanged conductance and an increased capacitance. (b) At low frequencies, the resultant output impedance is still a series *RC* circuit, but with an increased resistance and an increased capacitance.

an unchanged conductance of $g$ and a larger capacitance of $C_P+C'_{\rm ds}$, namely

$$Y'_{\rm out}\approx\left[Y_{O1}\left(\frac{C'_{\rm gd}}{C'_{\rm gs}+C'_{\rm gd}}\right)^2+g'_m\frac{C'_{\rm gd}}{C'_{\rm gs}+C'_{\rm gd}}\right]+\frac{1}{j\omega\left(\dfrac{C'_{\rm gs}C'_{\rm gd}}{C'_{\rm gs}+C'_{\rm gd}}+C'_{\rm ds}\right)}. \quad (17)$$

On the other hand, the total impedance $Z'_{\rm out}(=1/Y'_{\rm out})$ seen to the left-hand side of $R'_{\rm ds}$ at low frequencies is still a series *RC* circuit, but with a smaller resistance $r'$ equal to $r\cdot[C_S/(C_S+C'_{\rm ds})]^2$ and a larger capacitance equal to $C_S+C'_{\rm ds}$, namely

$$Z'_{\rm out}\approx\left(\frac{Z_{O1}}{1+g'_mZ_{O1}}+\frac{g'_m}{(Y_{O1}+g'_m)^2}\cdot\frac{C'_{\rm gs}}{C'_{\rm gd}}\right)\cdot\left(\frac{(1+g'_mZ_{O1})C'_{\rm gd}}{(1+g'_mZ_{O1})C'_{\rm gd}+C'_{\rm ds}}\right)^2+\frac{1}{j\omega\Big[(1+g'_mZ_{O1})C'_{\rm gd}+C'_{\rm ds}\Big]}. \quad (18)$$

Both situations are illustrated in Fig. 10(a) and (b), respectively. Consequently, the effect of $C'_{\rm ds}$ on the kink point is to move the prior intercept point to a new position determined by the unchanged constant conductance $g$ circle and the smaller constant resistance $r'$ circle. Therefore, the kink effect becomes more obscured when $C'_{\rm ds}$ is increased, as shown in Fig. 11. This is another reason why it is much easier to see the kink effect in bipolar transistors, especially in HBTs, as shown in Fig. 1, than in FETs because $C'_{\rm Ce}$ in bipolar transistors is usually much smaller than $C'_{\rm ds}$ in FETs.

We may now apply the previous conclusions to the case of large-size FETs. Obviously, if the device size of an FET is increased, its $g'_m$ increases accordingly, and from previous discussions, we predict that the kink phenomenon should become more visible. This is indeed the case, as shown in Fig. 4, where the size of a submicrometer gate GaAs FET was changed from 0.5 to 4 mm and $S_{22}$ was calculated by (1)–(9) with all the extrinsic elements taken into account. Note that the calculated values we obtained are almost identical with the data published by Aoki and Hirano [5], which are also shown in Fig. 4. The calculated values of the other three $S$-parameters ($S_{11}$, $S_{21}$, and $S_{12}$), though not shown here, were also in good agreement

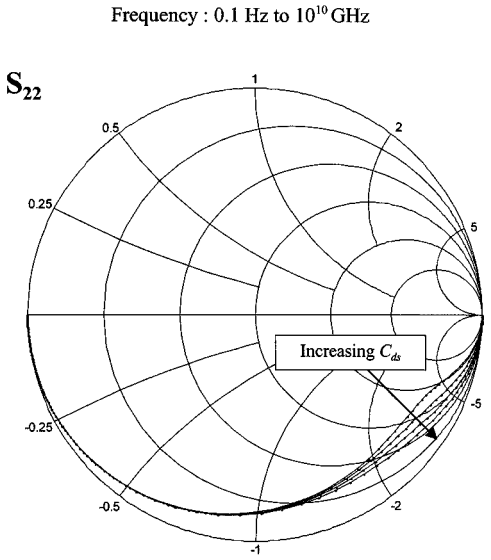


Fig. 11. Effect of $C'_{\rm ds}$ on the kink phenomenon of $S_{22}$. The kink phenomenon becomes increasingly obscured as $C'_{\rm ds}$ is increased because the intercept point of the constant resistance circle and the constant conductance circle moves to a new intercept point with a smaller resistance and an unchanged conductance.

with the experimental data. The excellent agreement between the calculated values and experimental data justifies our proposed theory. Although $C'_{\rm ds}$, $C'_{\rm gd}$, and $C'_{\rm gs}$ increase with device size as well, from (15) and (16), their effect on $r$ and $g$ cancel each other because they all increase by the same factor. Therefore, $g'_m$ is the dominant factor that changes the position of the intercept point or kink point.

It is also interesting to note the behavior of $S_{11}$ at low frequencies. If the effect of $C'_{\rm ds}$ is negligible, then from (10) $Z_{{\rm in},M}$ becomes a series *RC* circuit with a capacitance $C_M = (1 + g'_m R_L)C'_{\rm gd}$ (Miller capacitance) and a resistance $R_M = R_L/(1 + g'_m R_L)$, where $R_L = R'_{\rm ds} \| (R_d + Z_O)$. Therefore, $Z_{{\rm in},i}$ is a parallel combination of two series *RC* circuits, as shown in Fig. 12. At low frequencies, $Z_{{\rm in},i}$ can be represented by a series *RC* circuit with a total resistance and capacitance given by

$$Z_{{\rm in},i} = R'_i \cdot \left(\frac{C'_{\rm gs}}{C'_{\rm gs}+C_M}\right)^2 + R_M \cdot \left(\frac{C_M}{C'_{\rm gs}+C_M}\right)^2 + \frac{1}{j\omega(C'_{\rm gs}+C_M)}. \quad (19)$$

Therefore, the input impedance $Z_{\rm in} = R_g + Z_{{\rm in},i}$ of an FET is given by

$$Z_{\rm in} = R_g + (R_i + R_S) \cdot \left(\frac{C'_{\rm gs}}{C'_{\rm gs}+C_M}\right)^2 + R_M \cdot \left(\frac{C_M}{C'_{\rm gs}+C_M}\right)^2 + \frac{1}{j\omega(C'_{\rm gs}+C_M)}. \quad (20)$$

From (20), $S_{11}$ should follow a constant resistance circle at low frequencies which is evident from the experimental data in Fig. 3. Note the traditional estimated value $R_g + R_i + R_S$ [3], [6] of the real part of $Z_{\rm in}$ is a special case of our formula if $C_M = (1 + g'_m R_L) \cdot C'_{\rm gd} \ll C'_{\rm gs}$ is satisfied.

One additional advantage of our theory is that it provides a handy way to extract the device equivalent circuit parameters

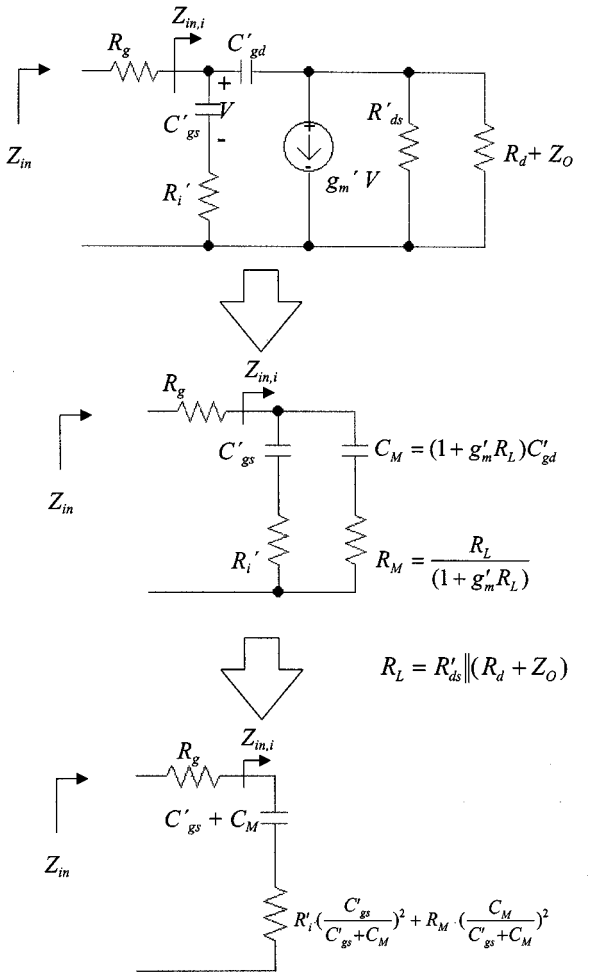


Fig. 12. Equivalent circuit of the input impedance at low frequencies if $C'_{\rm ds}$ is negligible.

from the measured $S$-parameters *at low frequencies*. The extraction procedure of the device parameters is detailed in the following. First, we assume that the parasitic access resistances $R_g$, $R_d$, and $R_s$ can be obtained by other separate measurements. $R_{\rm ds}$ can easily be read from the starting point of the measured $S_{22}$ at low frequency (typically 50 MHz) in the Smith chart, as was illustrated in Fig. 6. At low frequencies, (13) for $S_{12}$ can be approximated by

$$S_{12} = 2 \cdot sC'_{\rm gd} \cdot Z_O. \quad (21)$$

Therefore, $C_{\rm gd}$ can easily be determined from the measured $S_{12}$ according to (6) and (21). At low frequencies, (12) for $S_{21}$ approaches

$$S_{21} = -2 \cdot g'_m \cdot R_L \cdot \frac{Z_O}{Z_O + R_d}. \quad (22)$$

From the above expression and (7), $g_m$ can be obtained. From measured $S_{22}$ and $R_{\rm ds}$ and $R_d$, the impedance $Z'_{\rm out}$ seen to the left-hand side of $R'_{\rm ds}$ can be calculated. According to (4) and (18), the value of $C_{\rm ds}$ can be determined by observing how the imaginary part of $Z'_{\rm out}$ varies with frequency. Similarly, from

TABLE I
COMPARISON BETWEEN THE EXTRACTED VALUES OF THE DEVICE PARAMETERS OF A 0.25-$\mu$m-GATE SILICON n-MOSFET

| Frequency range 50MHz ~ 500MHz | Extracted Value | Exact Value | Error Percentage |
|---|---|---|---|
| $\mathbf{R_{ds}}$ **(Ω)** | 175.5 | 183 | -4.1% |
| $\mathbf{C_{gd}}$ **(fF)** | 42.6 | 41 | +3.9% |
| $\mathbf{C_{ds}}$ **(fF)** | 100.5 | 106 | -5.2% |
| $\mathbf{C_{gs}}$ **(fF)** | 270.5 | 280 | -3.4% |
| $\mathbf{R_i}$ **(Ω)** | 0* | 0 | |

*The extracted value is negative but since $R_i$ cannot be negative, zero is estimated.

measured $S_{11}$, the value of $C_{\rm gs}$ can be obtained according to (2), (11), (19), and (20). Finally, the value of $R_i$ is determined from the real part of $Z_{\rm in}$ in (20).

The extracted device equivalent-circuit parameters of a 0.25-$\mu$m MOSFET [4] according to the above-mentioned procedure are listed in Table I. The exact values are also listed in Table I for comparison. As can clearly be seen, the error percentage is satisfactorily small if we consider how simple this procedure is. The results of our parameter-extraction method can provide a good initial guess for further computer optimization.

## IV. CONCLUSIONS

In this paper, a novel theory based on dual-feedback circuit methodology has been proposed to calculate the transistor $S$-parameters. The calculated values agree excellently with experimental data. Our model not only calculates the $S$-parameters accurately, but also explains the origin of the kink phenomenon of $S_{22}$ in a Smith chart. The effect of $g_m$, $R_{\rm ds}$, $C_{\rm gs}$, $C_{\rm gd}$, and $C_{\rm ds}$ on the kink phenomenon can easily be deduced by our theory. It is found that the output impedance intrinsically behaves as a *series RC* circuit at low frequencies and as a *parallel RC* circuit at high frequencies. It is this inherent ambivalent characteristic of the output impedance that causes the kink phenomenon. Traditional two-port $Z$- or $Y$-parameters, though being very useful in calculating $S$-parameters, can hardly explain the behavior of $S$-parameters or give insight into the physical meaning of the $S$-parameters. A simple method for extracting transistor equivalent-circuit parameters from measured $S$-parameters has also been proposed based on our theory.

## REFERENCES


[1] B. Bayrajtariglu, N. Camilleri, and S. A. Lambert, "Microwave performance of n-p-n and p-n-p AlGaAs/GaAs heterojunction bipolar transistors," *IEEE Trans. Microwave Theory Tech.*, vol. 36, pp. 1869–1873, Dec. 1988.

[2] P. R. Gray and R. G. Meyer, *Analysis and Design of Analog Integrated Circuits*. New York: Wiley, 1993, pp. 579–584.

[3] R. A. Minasian, "Simplified GaAs M.E.S.F.E.T. model to 10 GHz," *Electron. Lett.*, vol. 13, no. 18, p. 549, 1977.

[4] Y. J. Chan, C. H. Huang, C. C. Weng, and B. K. Liew, "Characteristics of deep submicromenter MOSFET and its empirical nonlinear RF model," *IEEE Trans. Microwave Theory Tech.*, vol. 46, pp. 611–615, May 1998.

[5] Y. Aoki and Y. Hirano, "High-Power GaAs FETs," *High Power GaAs FET Amplifiers*, p. 81, 1993.

[6] M. Fukuta and Y. Hirachi, *Fundamentals of GaAs Field Effect Transistors* (in Japanese). Tokyo, Japan: Electron. Information Commun. Soc., 1992, p. 81.


**Shey-Shi Lu** (S'89–M'91–SM'99) was born in Taipei, Taiwan, R.O.C., on October 12, 1962. He received the B.S. degree from the National Taiwan University, Taiwan, R.O.C., in 1985, the M.S. degree from Cornell University, Ithaca, NY, in 1988, and the Ph.D. degree from the University of Minnesota at Minneapolis-St. Paul, in 1991, all in electrical engineering. His M.S. thesis was related to the planar doped barrier hot electron transistor, while his doctoral dissertation concerned the uniaxial stress effect on the AlGaAs/GaAs quantum well/barrier structures.

In August 1991, he joined the Department of Electrical Engineering, National Taiwan University, where he is currently a Professor. His current research interests are in the areas of radio-frequency integrated circuit (RFIC)/monolithic microwave integrated circuits (MMICs), and micromachined RF components.

**Chinchun Meng** received the B.S. degree in electrical engineering from the National Taiwan University, Taipei, Taiwan, R.O.C., in 1985, and the Ph.D. degree in electrical engineering from the University of California at Los Angeles, in 1992. His doctoral dissertation concerned the first continuous wave (CW) operation of multiquantum-well IMPATT oscillator at 100 GHz.

In 1993, he joined the Hewlett-Packard Component Group, Santa Clara, CA, as a Member of Technical Staff. His area of research and development has included HBT, MESFET and pseudomorphic high electron-mobility transistor (pHEMT) for microwave and RF power-amplifier application. He is currently an Associate Professor in the Department of Electrical Engineering, National Chung-Hsing University, Taichung, Taiwan, R.O.C. He is currently largely involved in power device and circuit for wireless communication. His research and publications are in the field of microwave circuits and semiconductor devices.

**To-Wei Chen** was born in Taiwan, R.O.C., on June 7, 1978. He is currently working toward the electrical engineering degree at the National Taiwan University, Taipei, R.O.C.

His current interest is in the area of telecommunication, especially in RFICs and MMICs.

**Hsiao-Chin Chen** was born in Taichung, Taiwan, R.O.C., on October 6, 1976. She received the B.S. degree in electrical engineering from the National Taiwan University, Taiwan, R.O.C., in 1998, and is currently working toward the M.S. degree in electrical engineering at the National Taiwan University.

Her research is focused on the design of RFICs and the related micromachining topics for wireless communication.